analytical chemistry

Article

pubs.acs.org/ac

Characterization of Solute Distribution Following Iontophoresis from a Micropipet

Douglas C. Kirkpatrick,[†] Martin A. Edwards,[†] Paul A. Flowers,[§] and R. Mark Wightman*[,†,‡]

[†]Department of Chemistry and [‡]Department of Chemistry and Neuroscience Center, University of North Carolina at Chapel Hill, Chapel Hill, North Carolina 27599-3290, United States

[§]Department of Chemistry and Physics, University of North Carolina at Pembroke, Pembroke, North Carolina 28372, United States

Supporting Information

ABSTRACT: Iontophoresis uses a current to eject solution from the tip of a barrel formed from a pulled glass capillary and has been employed as a method of drug delivery for neurochemical investigations. Much attention has been devoted to resolving perhaps the greatest limitation of iontophoresis, the inability to determine the concentration of substances delivered by ejections. To further address this issue, we evaluate the properties of typical ejections such as barrel solution velocity and its relation to the ejection current using an amperometric and liquid chromatographic approach. These properties were used to predict the concentration distribution of ejected solute that was then confirmed by fluorescence microscopy. Additionally, incorporation of oppositely charged fluorophores into the barrel investigated the role of migration on the mass transport of an ejected species. Results indicate that location relative to the barrel tip is the primary influence on the distribution of ejected species. At short distances (<100 μm), advection from electroosmotic transport of the barrel solution may significantly contribute to the distribution, but this effect can be minimized through the use of low to moderate ejection currents. However, as the distance from the source increases (>100 μm), even solute ejected using high currents exhibits diffusion-limited behavior. Lastly a time-dependent theoretical model was constructed and is used with experimental fluorescent profiles to demonstrate how iontophoresis can generate near-uniform concentration distributions near the ejection source.

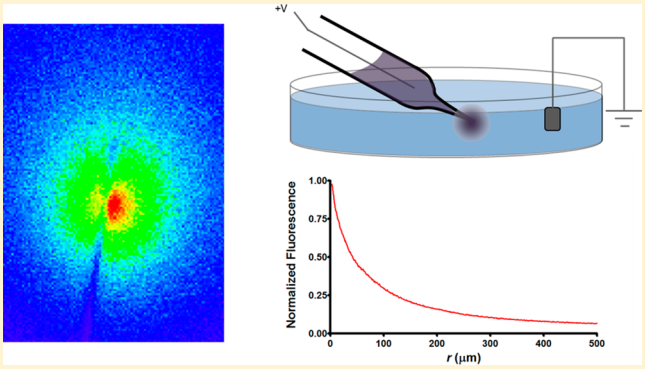

Iontophoresis is a drug delivery mechanism that uses a controlled current to eject solute from the tip of a pulled glass capillary. It was first utilized as a method to administer acetylcholine at a neuromuscular junction and was eventually adopted for a similar purpose at synaptic sites.[1,2] This technique has proved beneficial for applications in neuroscience as it provides several distinct advantages over more traditional methods of drug delivery, including local and rapid application, bypassing of the blood brain barrier, and avoiding interference with the behavior of animals.[3−6]

Iontophoresis has proved useful in modern studies as a tool to investigate a host of neurological properties such as receptor dynamics and location.[7−10] Despite its advantages, more widespread adoption of iontophoresis has been limited due to the inability to monitor and quantify ejections.[5,11,12] This has been partially addressed through various measurement strategies including electrochemical, radiometric, and fluorescent techniques.[13−16] Notably the addition of a carbon fiber to an adjacent barrel on the iontophoresis probe allows for the electrochemical detection of an electroactive solute while also providing an estimate of the ejection quantity.[17−19] However, obtaining precise drug concentrations from iontophoretic ejections remains difficult.[9]

While much of the attention regarding the quantification of iontophoresis has focused on ejection amount, the spatial distribution of ejected solute plays an equally important role on establishing the concentration of a delivered species. In contrast to pressure-based ejections, the electric field induced by the ejection current has been posited to facilitate electroosmosis in the tissue surrounding the ejection point.[20,21] However, this view is not shared by some who argue that the current density outside the barrel is too low to significantly contribute to mass transport.[22] In either case, the velocity of the ejected barrel solution may also be sufficient to displace previously delivered solute, adding an advective component to the mass transport. This is made possible by the presence of electroosmosis within the barrel, resulting in the transport of bulk solution from the tip.[16,23,24] Migration of charged ions within the barrel can also play an important role on the ejection rate.[25] However, a drop in the current density outside the barrel also raises questions regarding the influence of charge on the mass transport of ions following ejection.

Received: July 15, 2014
Accepted: August 26, 2014
Published: August 26, 2014

   dx.doi.org/10.1021/ac5026072 | *Anal. Chem.* 2014, 86, 9909−9916

In this study we establish the velocity range for iontophoretic ejections from barrels formed from micropipets and use these values to predict how advection affects the distribution of an ejected species. Concentration distributions are derived from steady state fluorescence measurements and were compared with the theoretical predications. Additionally, the effect of migration on the solute distribution was examined by comparing fluorescence intensity profiles of oppositely charged fluorophores. Finally, we constructed a simple model to approximate the concentration during and following an iontophoretic ejection. This model was used with experimental measurements to aid in the design of more effective protocols for iontophoretic experiments.

THEORY

To predict the distribution of substances ejected by iontophoresis from micropipets, we used a mathematical model to describe this process once steady state had been achieved. We assumed the ejected species is a neutral substance transported by convection and diffusion only. The source was assumed to be a sphere of radius a, and mass transport was considered to be spherically symmetric, with r as the radial coordinate and the origin at the center of the sphere. Lastly, the concentration was presumed to go to zero at distances far from the source. The differential equation to be evaluated is

$$J = C(r)v(r) - D\nabla C(r) \tag{1}$$

where J is the flux of the ejected species, C is its concentration, v is the radial velocity of the solution, and D is the diffusion coefficient. We define V as the volume flow rate from the barrel which gives

$$v(r) = V/4\pi r^2 \tag{2}$$

We only consider the solution at steady state requiring evaluation of

$$0 = \frac{\partial C(r)}{\partial t} = D\frac{\partial^2 C(r)}{\partial r^2} + \frac{\partial C(r)}{\partial r}\left(\frac{2D}{r} - \frac{V}{4\pi r^2}\right) \tag{3}$$

Introducing the dimensionless distance ρ ($\rho = r/a$), this can be written using the Peclet number in a similar manner to Weber and co-workers:[21]

$$\frac{dC(\rho)}{d\rho}\left(\frac{Pe}{\rho^2} - \frac{2}{\rho}\right) = \frac{d^2C(\rho)}{d\rho^2} \tag{4}$$

where the Peclet number (Pe) is a dimensionless value, which for the present work is given by

$$Pe = \frac{V}{4\pi aD} \tag{5}$$

This equation was solved previously using the boundary conditions that $C(\rho \to \infty) = 0$ and $J(\rho = 1)$ are constant. The solution is then

$$C(\rho) = \frac{J_0 a}{PeD}\left[1 - \exp\left(\frac{-Pe}{\rho}\right)\right] \tag{6}$$

where the flux at the boundary of the sphere, J_0, can be described by

$$J_0 = \frac{C_{int}V}{4\pi a^2} = \frac{DC_{int}Pe}{a} \tag{7}$$

where C_{int} is the concentration of the ejected substance in the interior of the barrel. Substitution of this value into the previous equation yields

$$C(\rho) = C_{int}\left[1 - \exp\left(\frac{-Pe}{\rho}\right)\right] \tag{8}$$

At small values of Pe (mass transport dominated by diffusion) this relationship collapses to

$$C(\rho) = \frac{C_{int}Pe}{\rho} \tag{9}$$

that can be rewritten as

$$C(r) = \frac{C_{int}V}{4\pi D}\left(\frac{1}{r}\right) \tag{10}$$

This equation reveals that, with $Pe \ll 1$, normalized concentration responses should superimpose and have shapes that are independent of a and are linear with $1/r$.

EXPERIMENTAL SECTION

Chemicals and Solutions. All chemicals were used as received from Sigma-Aldrich (St. Louis, MO) unless otherwise noted. Artificial cerebral spinal fluid (aCSF) was prepared with 126 mM NaCl, 2.5 mM KCl, 1 mM NaH_2PO_4, 26 mM $NaHCO_3$, 1.2 mM $MgCl_2$, 2.4 mM $CaCl_2$, and 11 mM glucose in deionized water with the pH adjusted to 7.4 using HCl. Fluorophore stock solutions were 10 mM for disodium fluorescein, tris(2,2′-bipyridyl)dichlororuthenium(II) ($Ru(bpy)_3Cl_2$), and rhodamine B, all in 5 mM NaCl. The stock of 7-amino-4-methylcoumarin (coumarin 120) was a saturated solution that was prepared by stirring with low heat for 20 min, resulting in a concentration near the solubility limit (low millimolar).[26] Before addition to the iontophoresis barrel, all stock solutions were diluted 1:1 with 5 mM NaCl and filtered using a 0.20 μm PTFE filter (EMD Millipore, Billerica, MA).

Iontophoretic Ejections. Iontophoresis probes were fabricated from four-barreled prefused glass (Friedrich & Dimmock, Millville, NJ) as previously described.[8,23] One barrel contained a carbon fiber for electrochemical measurements. To minimize natural convection during imaging, iontophoretic ejections were made into a 1% (wt/vol) agarose block (Promega, Madison, WI) prepared with aCSF. Low percentage agarose was used to minimize its hydraulic permeability.[27] The agarose (~2 cm thickness) was placed on a glass coverslip inside a rectangular barrier of Vaseline which contained aCSF. A Ag/AgCl pellet reference (World Precision Instruments, Sarasota, FL) was placed within the barrier to support the iontophoretic current. Using a micromanipulator, the tip of the iontophoresis barrel was carefully inserted into the agarose until it was approximately 500 μm beneath the surface. Ejections were initiated using a homemade current source (UNC Electronics Facility, Chapel Hill, NC) and controlled with customized software.

Amperometry and Liquid Chromatography. Ejections of 20 mM hydroquinone in 5 mM NaCl were performed into 1.5 mL Eppendorf polyethylene test tubes containing 100 μL aliquots of phosphate buffered saline (140 mM NaCl, 3 mM KCl, 10 mM NaH_2PO_4) adjusted to pH 7.4 with 3 M NaOH. The carbon fiber was used for amperometric oxidation of ejected hydroquinone at +0.9 V relative to a Ag/AgCl reference with a UEI current transducer (UNC Chemistry Electronics

dx.doi.org/10.1021/ac5026072 | Anal. Chem. 2014, 86, 9909−9916

Facility, Chapel Hill, NC). The amperometric current was integrated with respect to time to determine the total amount detected electrochemically by Faraday's law. The amount of hydroquinone that was not amperometrically oxidized was determined using liquid chromatography (HP series 1050, Hewlett-Packard, Palo Alto, CA). Injections (20 μL) were made onto a C18 reverse phase column (5 μm, 4.6 mm × 250 mm, Phenomenex, Torrance, CA) with a mobile phase consisting of 100 mM citric acid, 1 mM sodium hexyl sulfate (Research Plus, Barnegat, NJ), and 0.1 mM EDTA (pH = 3), with 10% added MeOH. Amperometric detection at the end of the column employed a glassy carbon thin layer radial cell (Bioanalytical Systems, West Lafayette, IN) held at +0.8 V relative to a Ag/AgCl reference. Data were recorded on customized LabVIEW software (Jorgenson Lab, UNC) using home-built electronics. The number of moles injected for each sample was determined by integration of the peak area and comparison to similarly prepared standards.

Fluorescence Measurements. Epifluorescence microscopy was performed using an Eclipse FN1 microscope (Nikon Instruments) with illumination from a Xenon halide source (X-Cite 120, EXFO). Filter cubes (Nikon Instruments) were used to select excitation and emission wavelengths specific to each fluorophore. Images were captured using a Retiga Exi camera (QImaging, Surrey, BC, Canada) and recorded with QCapture software (QImaging). For confocal imaging, an SP2 Laser Scanning Confocal Microscope (Leica, Wetzlar, Germany) was used with assistance from the Michael Hooker Microscopy Facility at the University of North Carolina Chapel Hill.

Data Analysis. To obtain fluorescence intensity-distance profiles for ejections performed on the epifluorescence setup, images were analyzed using a custom Matlab script (Figure 1A). Overlaid on the fluorescence intensity are 11 cross sections (dashed lines) that span outward from the tip of the iontophoresis barrel at 30° intervals. The twelfth cross-section nearest the barrel was omitted due to optical distortion. The fluorescence intensity along each line was subtracted from the background and averaged together, resulting in the final distribution profile for the ejection (Figure 1B). For ejections on the confocal microscope a similar analysis was employed that utilized the microscope associated software (LAS-AF lite v 2.6, Leica, Wetzal, Germany).

Brain Slice Experiments. Coronal brain slices of the dorsal striatum from male Sprague−Dawley rats were prepared. The animal was anesthetized with urethane (1.5 g/kg) and decapitated. Following immediate removal of the brain and immersion into oxygenated (95% O_2/5%CO_2) chilled aCSF, a vibratome (VF-200, Precisionary Instruments, San Jose, CA) was used to cut 300 μm thick sections. The slices were stored at room temperature in oxygenated aCSF and transferred to a perfusion chamber (RC-22, Warner Instruments, Hamden, CT) for measurements during perfusion with a constant stream of oxygenated aCSF at 37 °C. The iontophoresis barrel was placed just below the surface of the cortex where the tissue contrast was determined to be most uniform. During ejections, the perfusion was temporarily stopped. Animal procedures were approved by the Institutional Animal Care and Use Committee at the University of North Carolina at Chapel Hill. Special care was taken to reduce the number of animals used for this study and to minimize any suffering.

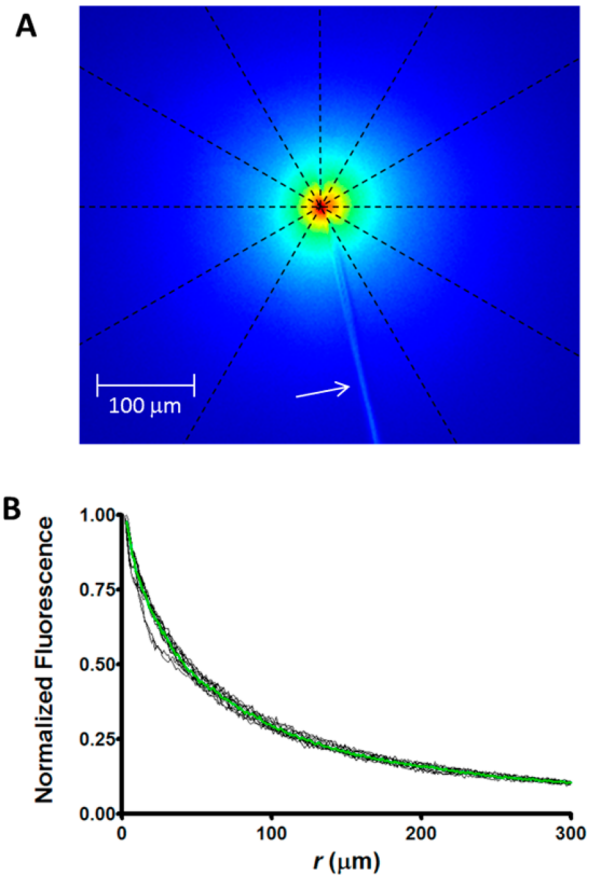

Figure 1. Determination of fluorophore distribution for iontophoretic ejections: (A) Matlab false color plot of fluorescence intensity for an ejection of fluorescein into 1% agarose. The dashed black lines depict 11 cross sections which extend from the origin at 30° intervals along which the intensity was recorded. The iontophoresis barrel is indicated by an arrow. (B) Background subtracted fluorescence intensity versus distance along each cross section (black) and average trace of all cross sections (green).

RESULTS AND DISCUSSION

Range of Ejection Velocities. To compare our experimental results to the theory, we needed to know the iontophoretic ejection velocities due to electroosmosis so that the Peclet numbers could be evaluated. To accomplish this, hydroquinone, a neutral molecule, was ejected into 100 μL aliquots of PBS. A carbon fiber on an attached barrel was used to quantify and monitor the ejection by amperometric oxidation (Figure 2A). The amount of hydroquinone oxidized by the carbon fiber, N, was determined by Faraday's law, $N = (Qn/F)$, where n is the number of electrons (2) transferred in the oxidation step and F is Faraday's constant. The charge Q was determined from integration of the oxidation current with respect to time. The amount of hydroquinone ejected, but not oxidized and thus remaining in the PBS aliquot, was determined using liquid chromatography with comparison of peak area to known standards. The total number of moles of hydroquinone ejected was calculated as the sum of the moles oxidized at the carbon fiber and that determined by liquid chromatography. The collection efficiency, defined as the fraction of hydroquinone detected by the fiber compared to the total amount ejected, ranged from 18 to 60%. This value was dependent on the amount of hydroquinone ejected and varied between barrels. While each barrel showed a linear response of

dx.doi.org/10.1021/ac5026072 | Anal. Chem. 2014, 86, 9909−9916

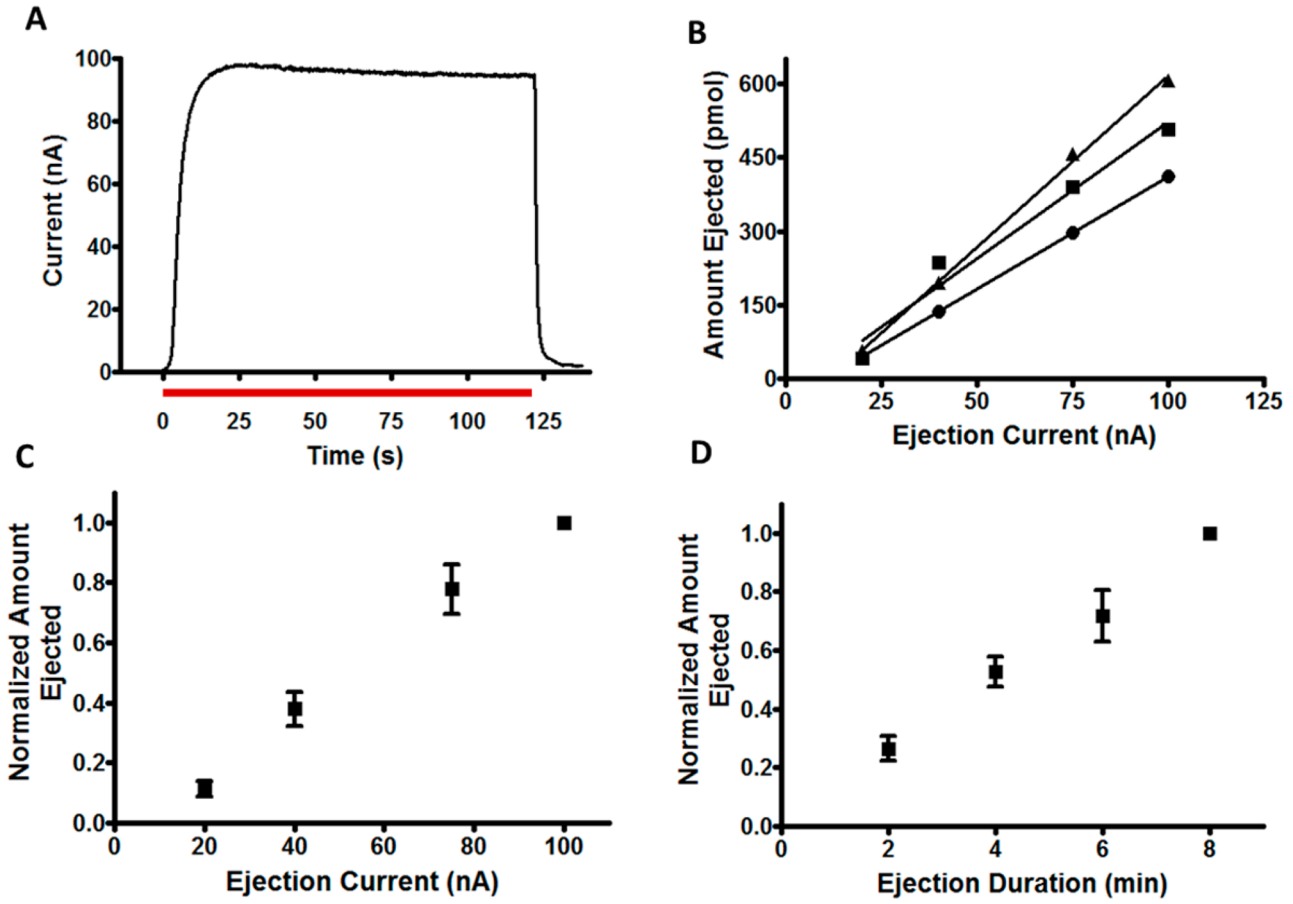

Figure 2. Determination of the velocity range for iontophoretic ejections: (A) Amperometric current versus time trace for a 2 min, 50 nA ejection of 20 mM hydroquinone in 5 mM NaCl into PBS. (Red bar represents ejection time) (B) Amount ejected versus ejection current for 3 min ejections of three different barrels. The ejection quantity is linear with ejection current, but the sensitivity varies between barrels. (C) Normalized amount of hydroquinone ejected versus ejection current for 3 min ejections (n = 5). Here and throughout the work error bars represent ±1 standard deviation. (D) Normalized amount of hydroquinone ejected versus ejection duration for 50 nA ejections (n = 5).

the amount ejected versus ejection current (3 min ejections), the sensitivity differed (Figure 2B). The amount of hydroquinone ejected from five barrels normalized to the amount ejected at 100 nA is plotted versus the magnitude of the ejection current in Figure 2C. This shows that an increase in the ejection current resulted in a proportional increase in the ejection amount, indicating the flux and ejection velocity of the barrel solution can be scaled by the ejection current. Further analysis of ejections in Figure 2C revealed that the volumetric flow rate was between 10 and 175 pL/s for ejection currents from 20 to 100 nA. Using this range, typical barrel dimensions (a = 0.5−1 μm) and a diffusion coefficient typical of small molecules we were ejecting (7.5×10^{-6} cm^2/s), eq 5 predicts Pe values between 1.1 and 37. We also examined the flux of ejections for different times (2−8 min) at a constant ejection current (50 nA). The amount of hydroquinone ejected normalized to the amount ejected in 8 min was linear with time, indicating a constant flux from the barrels (Figure 2D).

Effect of Velocity on Steady-State Distribution. To examine the concentration distribution at the tip of the iontophoresis barrel at different ejection rates, steady-state epifluorescence images of $Ru(bpy)_3^{2+}$ were recorded at different ejection currents. Steady state was achieved within 2−3 min. We confirmed that the epifluorescent microscope had sufficient depth of field for these measurements by comparing results with those obtained from a confocal microscope (see the Supporting Information). As the ejection current increased, so did the steady-state $Ru(bpy)_3^{2+}$ concentration using 4 min ejections (Figure 3A). Because of the higher ionic strength of the $Ru(bpy)_3^{2+}$ solutions that were used, it could support larger currents compared to barrels that contained neutral hydroquinone and 5 mM NaCl. The total fluorescence from $Ru(bpy)_3^{2+}$ within 500 μm of the barrel tip was determined by effective spherical integration of the concentration profiles, assuming spherical symmetry in nonimaged planes. These values were linear with ejection current when results were averaged from six barrels (Figure 3B). Once again there was linearity between the total amount and the ejection current, consistent with the previously established relationship between velocity and the ejection current.

If the diffusion-limited, steady-state condition is approached (Pe < 1), then the normalized concentration distribution should be independent of ejection velocity. To test this, the fluorescence curves from Figure 3A were normalized by the fluorescence intensity at a similar distance from the barrel and compared. When the amplitudes were normalized to their values measured 1 μm from the barrel tip, the distributions were similar at the lower range of ejection currents, the expected condition for small values of Pe (Figure 3C). However, at larger ejection currents the curves diverged. Under these conditions, advection from the velocity of the barrel solution is sufficient to move previously ejected solute,

dx.doi.org/10.1021/ac5026072 | Anal. Chem. 2014, 86, 9909−9916

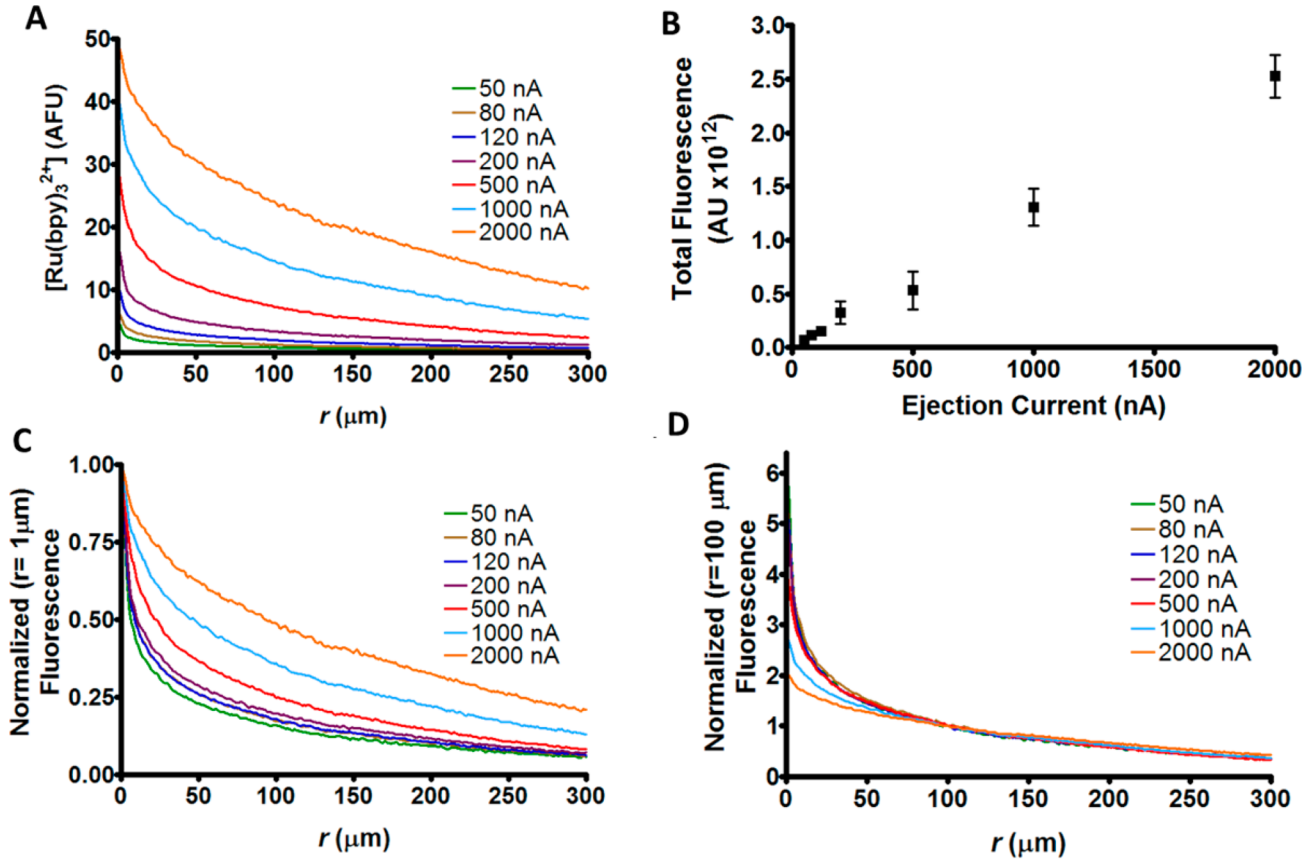

Figure 3. Fluorescence at steady state for ejections of 5 mM $Ru(bpy)_3^{2+}$ in 5 mM NaCl: (A) The steady-state fluorescence intensity for ejections ranging from 50 to 2000 nA. (B) The total fluorescence intensity of $Ru(bpy)_3^{2+}$ within 500 μm of the origin versus ejection current. Steady-state distributions (n = 7) were integrated about a sphere to determine the total fluorescence. (C) Steady-state fluorescence profiles from part A normalized at the ejection origin. (D) Steady-state fluorescence profiles from part A normalized at 100 μm from the origin.

indicating Pe > 1. The fluorescent measurements in agarose thus agree with the liquid chromatographic results that the Pe values are low for ejection currents <50 nA with the conditions employed.

To examine the impact of advection on the steady state distribution at distances further from the ejection origin, the distributions in Figure 3A were normalized by the intensity 100 μm from the barrel (Figure 3D). The close alignment of these curves demonstrates that advective convection has little effect on the distributions far from the origin. Although the normalization distance required to see a convergence varied, distributions obtained from other barrels (n = 7) behaved similarly when normalized within 100−200 μm of the tip (data not shown). Thus, even when Pe > 1, the total volume affected by an ejection at steady-state can be approximated independently of the ejection current using the apparent diffusion rate of the ejected species. Spherical integration of the intensity for normalized distributions displaying the smallest dependence on ejection current revealed that ∼10% of the ejected solute at steady state was within 100 μm of the barrel.

Effect of Molecular Charge on Steady State. To examine whether the molecular charge of an ejected species influences the concentration distribution using solutions that approximate physiological conditions, steady state profiles of fluorophores with different charges were compared. The steady-state distributions of ejected fluorescein, rhodamine B, coumarin 120, and $Ru(bpy)_3^{2+}$, which possess charges at pH 7.4 of 1−, 0, 0, and 2+, respectively, overlay when normalized by the intensity 30 μm from the barrel (Figure 4A). These measurements are the average from at least 12 barrels for each compound. Clearly, the differently charged fluorophores have similar concentration distributions, indicating that mass transport by migration away from the barrel tip does not play a role under these conditions. Additionally, ejections from barrels containing multiple fluorophores showed no difference in the steady-state distribution when each was separately imaged (data not shown).

In these experiments, the normalization distance of 30 μm was selected to minimize errors in specifying the center of the ejection that often was distorted by the carbon fiber. There also exists the possibility of fluorophore self-quenching, which would be most prevalent in the concentrated region near the origin. Additionally although these ejections employed moderate ejection currents (<85 nA), there is still an advective component that was previously shown to be minimized by normalization further from the origin. Lastly, Weber and co-workers showed that a zeta potential mismatch between the glass barrel and the surrounding medium can induce radial electroosmotic transport and increase the rate of mass transport of ejected solute.[21] To examine whether this was occurring in our gel, the zeta potential of the glass was altered by raising the ionic strength of the barrel solution. However, ejections performed of $Ru(bpy)_3^{2+}$ in 5 mM and 150 mM NaCl displayed no difference in the steady state conformation (see the Supporting Information), indicating that this additional electroosmotic force was not a factor within the agarose. Thus,

dx.doi.org/10.1021/ac5026072 | Anal. Chem. 2014, 86, 9909−9916

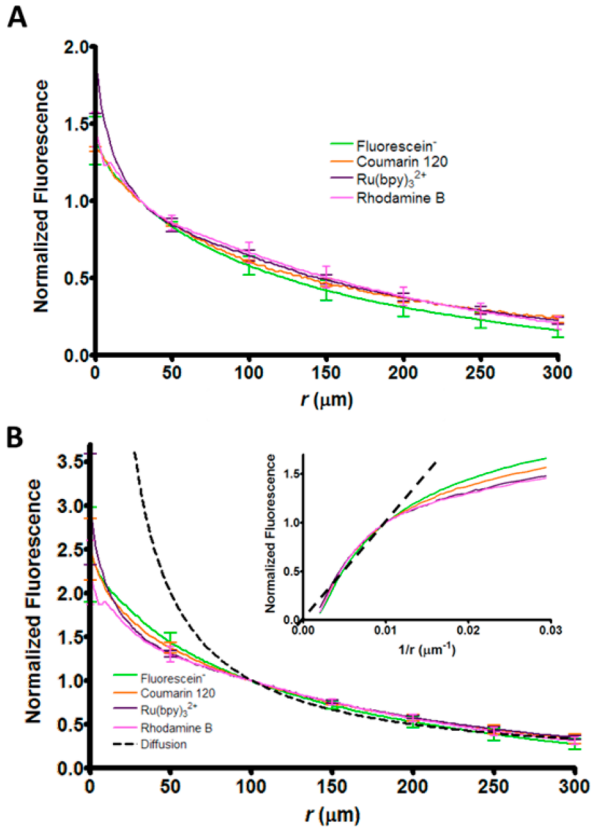

Figure 4. Effect of molecular charge on steady-state fluorescence distribution: (A) Average steady state fluorescence profiles (n = 12) normalized at 30 μm for $Ru(bpy)_3^{2+}$ (purple), coumarin 120 (orange), rhodamine B (pink), and fluorescein (green) into 1% agarose. (B) Comparison of steady-state distributions from part A to the diffusion-limited case (dashed) predicted by eq 10. A plot of the intensity versus $1/r$ (inset) highlights the transition to diffusion-limited behavior away from the origin.

we conclude that under the conditions used in this work, migration away from the barrel tip is minimized. However, both electroosmosis and migration contribute to the rate of ejection out of the barrel tip as shown previously.[23]

To examine further whether the steady-state profiles were diffusion-limited away from the origin, the fluorescence distributions were compared to a theoretical diffusion curve calculated from eq 10. In this case, the steady state distributions from Figure 4A and the $1/r$ curve were normalized 100 μm from the barrel (Figure 4B). Consistent with the fact that the experimental distributions were obtained with $Pe > 1$, there is a noticeable deviation from the diffusion-limited case near the ejection origin. After the first 100 μm, however, the distribution follows the $1/r$ model. To highlight the transition to diffusion-limited transport, the curves were replotted on a $1/r$ axis, shown in the inset of Figure 4B. Here the distributions at distances further from the barrel ($0 < 1/r < 0.01$ μm^{-1}) are linear and track the diffusional result curve, demonstrating that mass transport of ejected solute >100 μm from the barrel is diffusion controlled.

Steady-State Ejections in Brain Slices. The steady-state distribution following ejections into brain tissue is expected to have differences from those measured in agarose due to different structural and electrical properties. Brain slices exhibit tortuosity in diffusion pathways that lowers the apparent diffusional rate.[28] Furthermore, as Weber demonstrated,[29] negative cellular membrane charge may introduce an additional electroosmotic component not present in the gel. Therefore, we made iontophoretic ejections of coumarin 120 (neutral) into the cortex of rat brain slices and compared the concentration profiles to ones obtained in agarose for the same substance (Figure 5A). When the fluorescence intensities

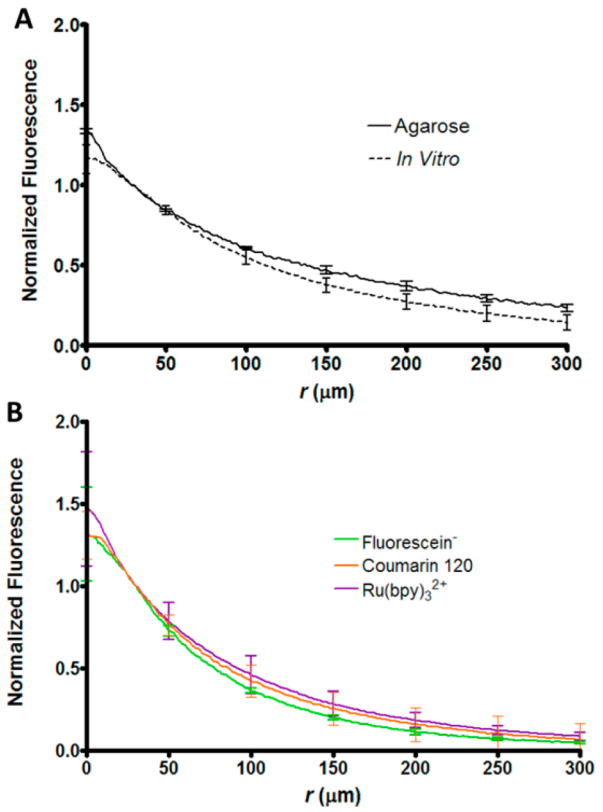

Figure 5. Fluorescence distribution for iontophoretic ejections into rat brain slices. To minimize Pe, ejections were performed using moderate ejection currents (<85 nA) and normalized 30 μm from the origin. (A) Comparison of the steady-state fluorescence intensity for ejections of coumarin 120 into agarose (solid, n = 12) and the rat cortex (dashed, n = 6). (B) Fluorescence intensity for fluorophores of different charges after 2 min ejections (n = 6) into the rat cortex. Similar to the ejections in agarose, different charge states [$Ru(bpy)_3^{2+}$ (2+), coumarin 120 (0), and fluorescein (1−)] had no effect on the distribution.

were normalized to the values 30 μm from the barrel origin, there was only a slight (but significant) difference between the profiles due to media (p = 0.027, two-way ANOVA). Similarly, the steady-state distribution of $Ru(bpy)_3^{2+}$ in a brain slice also showed only small differences to the responses in agarose (data not shown). To ensure that the molecular charge of an ejected species does not influence the distribution in brain slices, ejections of fluorescein were performed in brain slices and compared to the coumarin 120 and $Ru(bpy)_3^{2+}$ distributions in the same preparation (Figure 5B). As in the agarose gel, the distribution of any ejected species in brain tissue was not influenced by the charge.

Modeling of Time-Dependent Diffusive Distribution from an Iontophoretic Barrel. A description of the diffusion limited distribution was constructed in LabVIEW for spherically divergent diffusion using a convolution method established by Engstrom and co-workers.[30,31] From the step-response function for spherically divergent diffusion, the impulse response

dx.doi.org/10.1021/ac5026072 | Anal. Chem. 2014, 86, 9909−9916

function was derived, and it was convoluted with the Heavyside step function that approximates the flux at the origin. Using a time of 300 s to ensure steady state conformation, Figure 6A displays the convolved profile assuming a diffusion coefficient of 2.0×10^{-6} cm^2/s, lowered to account for slower diffusion in the brain.[28] The validity of the model is confirmed by the overlay of the $1/r$ diffusion curve from eq 10. To examine how the concentration will change over the time course of an ejection, ejections of 30, 60, and 300 s were simulated. The concentration 100 μm from the source is displayed in Figure 6B (lines), along with experimental data (dots) for $Ru(bpy)_3^{2+}$ fluorescence intensity. The point source model approximates the experimentally observed formation of a steady state and its relaxation when the ejection is terminated. Discrepancies may be explained by the minor advective component near the barrel that is unaccounted for in the diffusion model. This decreases the experimental rise time and alters the relaxation concentration due to differences in the steady-state distribution. During ejection, full steady state takes a long time to realize but reaches approximately 90% of its value within 100 μm after just 2 min. To visualize the spatial distribution after terminating an ejection, steady state was achieved with $Ru(bpy)_3^{2+}$ in agarose and the ejection current was disabled (Figure 6C). When the fluorescence data were plotted similarly to Figures 4 and 5 allowing time for relaxation from the steady state produced a more dilute and spatially uniform distribution. This experiment mimics the way iontophoresis has been used to introduce drugs to modulate dopamine release in the brain.[9] The drug is locally introduced by iontophoretic ejection, the concentrations are allowed to relax for a finite period (120 s in our published work), and then the dopaminergic neurons are stimulated. Changes in amplitude of the evoked release relative to a predrug release profile indicate the drug action.

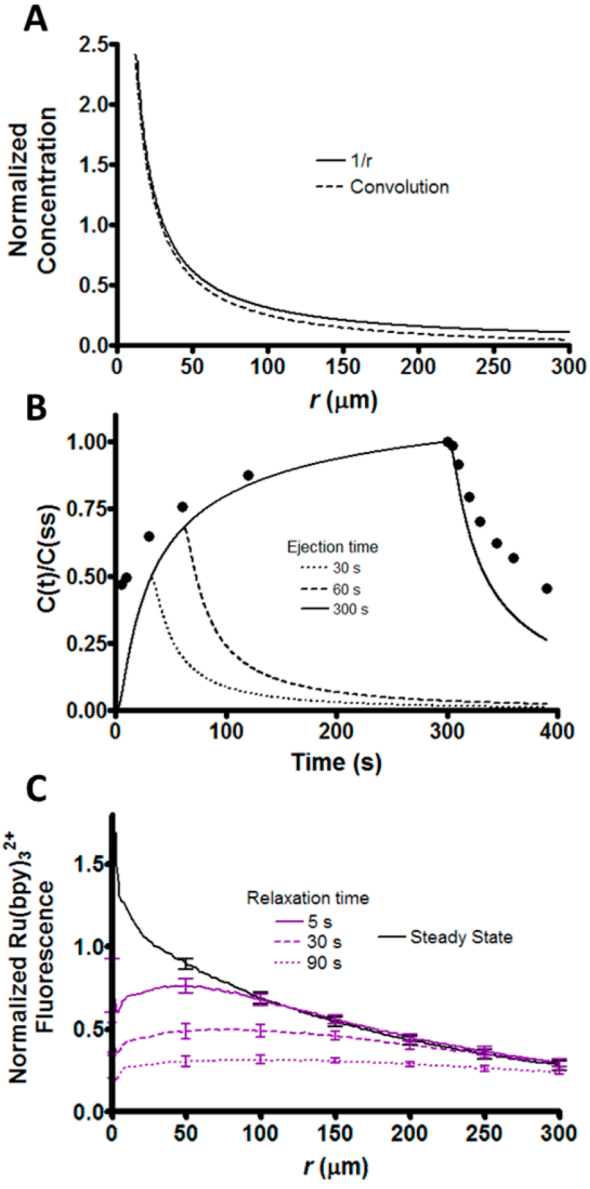

Figure 6. Time-dependent diffusion model and experimental applications. (A) Comparison of the 1/r curve from eq 10 (solid) with a model of spherically divergent diffusion (dashed) for a 300 s ejection. (B) Concentration 100 μm from the origin versus time for simulated iontophoretic ejections of 30 (dotted), 60 (dashed), and 300 s (solid). All concentrations were normalized by the value at 300 s. Experimental data (dots) show that the model approximates the observed behavior. (C) Average (n = 6) $Ru(bpy)_3^{2+}$ fluorescence distribution following termination of an ejection. Steady state was achieved in agarose (black) and the fluorescence intensity was recorded at 5 (purple, solid), 30 (purple, dashed), and 90 s (purple, dotted) after the ejection current was disabled. The intensity for each distribution was normalized by the intensity at steady state 30 μm from the barrel.

CONCLUSIONS

The velocity of solution ejected from the barrel scales proportionally with the ejection current. The impact of advection on the concentration distribution of solute from iontophoretic delivery has been demonstrated to be significant at high ejection currents but can be minimized by using low to moderate ejection currents. In any case the distribution of solute further from the origin (>100 μm) is much less impacted by advection and is primarily diffusion-limited. Additionally, for small molecules such as those considered in this work, the mass transport of an ejected ion is independent of charge in brain tissue, indicating that migration outside of the barrel does not play a role on solute distribution. Lastly, diffusional relaxation from steady state produces a near uniform concentration bolus within 90 s of terminating the ejection, demonstrating how iontophoresis may be incorporated in future applications for more accurate quantification.

ASSOCIATED CONTENT

Supporting Information

Additional detail is provided where noted. This material is available free of charge via the Internet at http://pubs.acs.org.

AUTHOR INFORMATION

Corresponding Author

*E-mail: rmw@unc.edu. Phone: (919) 962-1472.

Author Contributions

All authors have given approval to the final version of the manuscript.

Notes

The authors declare no competing financial interest.

ACKNOWLEDGMENTS

Dr. Michael Chua and Dr. Neal Kramarcy at the UNC Michael Hooker Microscopy Facility are acknowledged for their

assistance with confocal microscopy. Additionally, the UNC Department of Chemistry Electronics Facility and Collin McKinney contributed significantly through the construction of instrumentation and software for data acquisition. The Jorgenson lab at UNC also provided software for LC data acquisition and analysis. This research was supported by a grant from NIH (Grant DA010900). P.A.F. was supported by a Directed Academic Leave provided by the UNCP Office of Academic Affairs.

REFERENCES

(1) Hicks, T. P. *Prog. Neurobiol.* **1984**, *22*, 185−240.
(2) Del Castillo, J.; Katz, B. *J. Physiol.* **1955**, *128*, 157−181.
(3) Pierce, R. C.; Rebec, G. V. *Neuroscience* **1995**, *67*, 313−324.
(4) West, M. O.; Woodware, D. J. *J. Neurosci. Meth.* **1984**, *11*, 179−186.
(5) Bloom, F. E. *Life Sci.* **1974**, *14*, 1819−1834.
(6) Purves, R. *Trends Neurosci.* **1980**, *3*, 245−247.
(7) Overton, P.; Clark, D. *Synapse* **1992**, *10*, 131−140.
(8) Belle, A. M.; Owesson-White, C.; Herr, N. R.; Carelli, R. M.; Wightman, R. M. *ACS Chem. Neurosci.* **2013**, *4*, 761−771.
(9) Herr, N. R.; Daniel, K. B.; Belle, A. M.; Carelli, R. M.; Wightman, R. M. *ACS Chem. Neurosci.* **2010**, *1*, 627−638.
(10) Bucher, E. S.; Fox, M. E.; Kim, L.; Kirkpatrick, D. C.; Rodeberg, N. T.; Belle, A. M.; Wightman, R. M. *J. Cereb. Blood Flow Metab.* **2014**, *34*, 1128−1137.
(11) Purves, R. *J. Physiol.* **1980**, *300*, 72−73.
(12) Purves, R. *J. Theor. Biol.* **1976**, *67*, 789−798.
(13) Chen, K. C.; Nicholson, C. *J. Neurosci. Meth.* **2002**, *122*, 97−108.
(14) Dionne, V. E. *Biophys. J.* **1976**, *16*, 705−717.
(15) Purves, R. *J. Neurosci. Meth.* **1979**, *1*, 165−178.
(16) Bevan, P.; Bradshaw, C. M.; Pun, R. Y.; Slater, N. T.; Szabadi, E. *Experientia* **1981**, *37*, 296−297.
(17) Armstrong-James, M.; Millar, J. *Nature* **1980**, *288*, 181−183.
(18) Armstrong-James, M.; Fox, K.; Kruk, Z. L.; Millar, J. *J. Neurosci. Meth.* **1981**, *4*, 385−406.
(19) Kruk, Z. L.; Armstrong-James, M.; Millar, J. *Life Sci.* **1980**, *27*, 2093−2098.
(20) Trubatch, J.; Van Harreveld, A. *J. Theor. Biol.* **1972**, *36*, 355−366.
(21) Guy, Y.; Faraji, A. H.; Gavigan, C. A.; Strein, T. G.; Weber, S. G. *Anal. Chem.* **2012**, *84*, 2179−2187.
(22) Norman, R. S. *J. Theor. Biol.* **1975**, *52*, 159−171.
(23) Herr, N. R.; Kile, B. M.; Carelli, R. M.; Wightman, R. M. *Anal. Chem.* **2008**, *80*, 8635−8641.
(24) Bath, B. D.; Scott, E. R.; Phipps, J. B.; White, H. S. *J. Pharm. Sci.* **2000**, *89*, 1537−1549.
(25) Curtis, D. R. *Physical Techniques in Biological Research*; Academic Press: New York, 1964; p 55.
(26) Nowakowska, M.; Smoluch, M.; Sendor, D. *J. Incl. Phenom. Macro* **2001**, *40*, 213−219.
(27) Johnson, E. M.; Deen, W. M. *AIChE J.* **1996**, *42*, 1220−1224.
(28) Sykova, E.; Nicholson, C. *Physiol. Rev.* **2008**, *88*, 1277−1340.
(29) Xu, H.; Guy, Y.; Hamsher, A.; Shi, G.; Sandberg, M.; Weber, S. G. *Anal. Chem.* **2010**, *82*, 6377−6383.
(30) Engstrom, R. C.; Wightman, R. M.; Kristensen, E. W. *Anal. Chem.* **1988**, *60*, 652−656.
(31) Kawagoe, K. T.; Wightman, R. M. *Talanta* **1994**, *41*, 865−874.